J. Fluid Mech. (1990), *vol.* 221, *pp.* 183–204
Printed in Great Britain

Coalescence and separation in binary collisions of liquid drops

By N. ASHGRIZ AND J. Y. POO
Department of Mechanical and Aerospace Engineering, State University of New York at Buffalo, Buffalo, NY 14260, USA

(Received 27 November 1989)

An extensive experimental investigation of the binary collision dynamics of water drops for size ratios of 1, 0.75, and 0.5, for the Weber-number range of 1 to 100, and for all impact parameters is reported. Two different types of separating collisions, namely reflexive and stretching separations, are identified. Reflexive separation is found to occur for near head-on collisions, while stretching separation occurs for large-impact-parameter collisions. The boundaries between both of the separating collisions and coalescence collision are found experimentally. Theoretical models for predictions of the reflexive and stretching separation are also given.

1. Introduction

Collision dynamics of liquid drops is one of the most interesting yet very complicated problems in fluid dynamics. This phenomenon commonly occurs in atmospheric raindrop formation, and among dispersed phase systems such as in liquid–liquid extraction, emulsion polymerization, waste treatment and hydrocarbon fermentation (Shah *et al.* 1972; Park & Blair 1975). Recently, it has also been found to be important in dense spray systems, where drop collisions can significantly alter the spray characteristics, such as drop size and velocity distribution (O'Rourke & Bracco 1980).

Because of its complexity, the study of this three-dimensional free-surface flow problem has been mostly limited to experiments. Numerous experimental results on drop collision phenomenon have appeared in the literature, and a very complete review of these works up to 1970 is given by Park (1970). In fact Park's own work is perhaps the most complete investigation of the drop collision phenomenon up to the present. Also the recent book by Vasenin *et al.* (1986), published in Russian, refers to much of the Russian literature in this field. To name a few, early works by Gorbachev & Mustel (1935) and Gorbachev & Nikiforova (1935) report observations of the collision of a drop suspended at the end of a heavy pendulum or a slide with a stationary drop on a paraffin plate; Arkhipov, Vasenin & Trofimov (1983) have conducted a detailed cinematographic investigation of drop collisions.

A large group of investigations have considered the impact of a falling drop on a suspended or a half-drop, at different relative velocities and impact parameters, and for various ambient conditions (Schotland 1960; Jayaratne & Mason 1964; List & Whelpdale 1969). The collision outcomes of such experiments are significantly altered by the existence of the supporting systems. These problems are eliminated by using controlled collisions between pairs of drops in free flight. Such studies are exemplified by the works of Ryley & Bennet-Cowell (1967), Cotton & Gokhale (1967), Adam, Lindblad & Hendricks (1968), Brazier-Smith, Jennings & Latham (1972),

Levin, Neiburger & Rodriguez (1973), Bradley & Stow (1978, 1979), Arkhipov *et al.* (1983), Podvyotsky & Schraiber (1984), Ashgriz & Givi (1987), and Jiang, Umemura & Law (1990).

The major objectives of drop collision studies have been to answer the following questions: (*a*) what are the drop collision outcomes and their characteristics? (*b*) what parameters, and their values, define the boundaries between different types of collisions? Neither of the above questions have been fully answered up to this date. However, some generalized collision outcomes have been reported, which can be categorized into four different types, namely bouncing, coalescence, separation, and shattering collisions. In bouncing collision, contact of drop surfaces is prevented by the intervening gas film, and drops bounce apart. Coalescence collision refers to collisions in which two drops permanently combine and generate one single drop. Separation collision is when drops combine temporarily and later separate into a 'string' of two or more drops. And shattering collision, which is the characteristic of high-relative-velocity collision, is when drops disintegrate into a 'cluster' of many smaller droplets. In this paper we shall show that there are many sub-categories of drop collision within the above generalized ones and we shall discuss them based on the governing physical parameters.

As far as the boundaries between different types of collisions are concerned, only a few experiments have provided quantitative results. For instance, Adam *et al.* (1968) obtained the boundary between coalescence and separation for a pair of equal-size drops with 600 μm and 120 μm diameters. More detailed studies by Park (1970), Brazier-Smith *et al.* (1972), and Arkhipov *et al.* (1983) have been conducted on the collision of water drops with different size ratios. They have reported the critical parameters for which bouncing, coalescence, and separating collisions occur. More recently, Jiang *et al.* (1990) have completed an experimental investigation on the collision of normal-alkane drops. Their results show that the collision of alkane drops is significantly different than those of water drops. Because control and measurement of all the governing parameters in the collision phenomenon is a difficult task, some researchers have provided information on the probability of occurrence of a particular type of collision. For instance, Low & List (1982*a*, *b*), and Ashgriz & Givi (1989) have found the probability of coalescence, i.e. coalescence efficiency, for water and fuel drops respectively. In this paper we shall define the drop collision phenomenon in a more detailed and physically rational fashion, and provide quantitative boundaries between coalescence and separating collisions.

2. Experimental set-up

The technique used in our experiments is based on the collision of two uniform-size drop streams. A water jet is issued from a glass nozzle attached to a flattened aluminium tube with piezoelectric plates on its both sides. The piezoelectric plates, which are subject to a square wave with alternating voltage, expand and contract, disturbing the liquid jet. With careful control of the flow rate and the alternating frequency, the liquid jet is broken into a stream of uniform size drops. Steady flow of the liquid is obtained by using a pressurized tank. The pressure in the tank is controlled by a regulated nitrogen cylinder (for more details, see Ashgriz & Givi 1987; Poo 1989).

The two drop streams collide on a vertical plane and their collision dynamics are recorded by a video camera placed horizontally. It should be noted that the collision point of two streams has to be situated far downstream of the nozzle so that the

initial oscillatory motion of the drops is completely damped. The main measurement technique used in our experiments is flow visualization. Two different kinds of visualization are used, namely high-speed video and conventional video recording. The recording done by a high-speed video camera (Kodak EktaPro 1000 Motion Analyzer) is suitable for visualizing the evolution of colliding pair of drops. This camera is usually operated at 1000 frames per second. The recorded video pictures are viewed frame by frame, and the collision angle and the relative positions of the drops are measured.

The drop diameter, d, and velocity, u, are calculated by the following formulae:

$$d = \left(\frac{6q}{\pi f}\right)^{\frac{1}{3}}, \tag{1}$$

$$u = fs, \tag{2}$$

where s is the spacing between drops, measured from the video pictures, f is the alternating disturbance frequency, which also represents the frequency of drop generation, and q is the liquid flow rate, measured by a graduated cylinder.

The high-speed video camera is in black and white and it cannot provide any information on the mass transfer of the liquid during the collision process. Therefore, a conventional (30 frames per second) colour video camera is used to record the collision of coloured drops. In this case, both piezoelectric plates are connected to the same function generator, resulting in two synchronized drop streams. Each and every collision is then exactly the same as the previous one. This allows visualization of the collision phenomenon by the stroboscopic technique.

3. Description of the binary drop collision phenomenon

Consider two spherical liquid drops travelling in a gas medium. As the two drops approach each other, a gas layer may get trapped between them. Under certain conditions this compressed gas layer may prevent the contact of the drop surfaces, and so the drops deform and bounce apart. Bouncing collision is therefore dependent on the ambient gas characteristics, and its study will require quantification of the external parameters, such as the density of the surrounding gas, the flow field surrounding the drops, and the shape of the drops upon impact. Deformation and drainage of the gas film separating two drops has been the subject of many investigations, a recent review of which is given by Wasan & Malhotra (1986). Weinbaum, Chen & Ganatos (1989) have also provided an analysis of the collision and rebound of surfaces due to the fluid motion and pressure forces in the gap between them. In the present work no quantitative information on the external parameters is obtained, and therefore no attempt is made to correlate the bouncing collision data.

Generally, if the two drops do not bounce and their surfaces touch one of the following phenomena may occur. They may coalesce permanently; they may combine temporarily, and later separate into two or more drops; or they may shatter upon impact. The shattering collision occurs at high velocities where the surface tension forces are only of secondary importance, and the phenomenon is inertia dominated. Because of the limitations in our experimental set-up in generating high-velocity binary drop collisions, shattering collisions are not studied either. The main concern of this work is, therefore, coalescence and separating collisions.

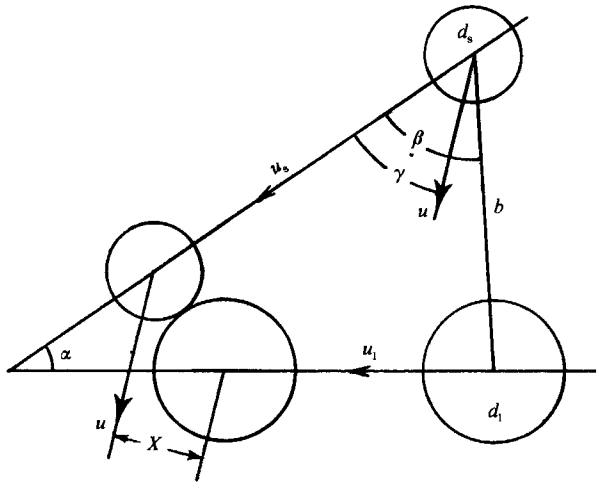

FIGURE 1. Schematic of the collision of two moving drops, with velocities u_l and u_s, diameters d_l and d_s, colliding with a collision angle of α, and an impact parameter X. The symbols used in this figure are defined in the text.

In the range of the parameters used in our experiments, the effects of the surrounding air on the collision outcome seem insignificant. Therefore, the phenomenon of binary drop collision can be described based on the liquid drop density ρ, viscosity μ, surface tension σ, the diameter and velocity of the larger drop d_l and u_l, and those of the smaller drop d_s and u_s. An important parameter governing the collision outcome is the relative velocity of the two drops. If the trajectories of the two drops form an angle α (see figure 1), called the collision angle, the relative velocity of the two drops will be equal to

$$u = (u_l^2 + u_s^2 - 2u_l u_s \cos\alpha)^{\frac{1}{2}}.$$

Another important parameter governing the collision phenomenon is the impact parameter, X, which is defined as the distance from the centre of one drop to the relative velocity vector placed on the centre of the other drop (see figure 1). By dimensional analysis the above parameters can be grouped into four dimensionless numbers. They are Reynolds number, Weber number, drop diameter ratio, and non-dimensional impact parameter, x, which are defined as follows:

$$Re = \frac{\rho d_l u}{\mu}, \quad We = \frac{\rho d_s u^2}{\sigma}, \quad \Delta = \frac{d_s}{d_l}. \quad x = \frac{2X}{d_l + d_s}.$$

In binary water-drop collisions with Reynolds numbers in the range of 500 to 4000, the range studied in this work, the Reynolds number does not seem to play a significant role on the outcome of the collision. Therefore, the main parameters that influence collision outcome are Weber number We, drop diameter ratio Δ, and impact parameter x.

Here, the collision outcome of drops for a wide range of Weber numbers, all possible impact parameters, and different size ratios are investigated. The Weber number is controlled by changing the relative velocity. The relative velocity is changed by adjusting the liquid flow rate, or by varying the collision angle, α. The drop diameters are controlled by the size of the glass nozzles. Five different nozzle

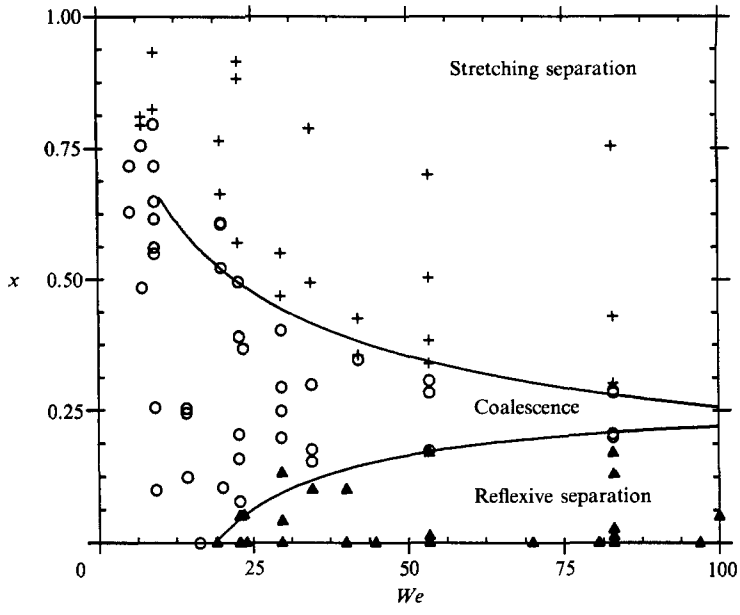

FIGURE 2. Analytically obtained regions of coalescence, reflexive separation, and stretching separation for drop size ratio $\Delta = 1.0$, together with experimental data (+, stretching separation; ○, coalescence; ▲, reflexive separation.

sizes are used: 100, 200, 300, 400, and 500 μm. They are combined to give diameter ratios from 0.5 to 1.0. The impact parameter is calculated by measuring the positions of two drops before collision and using the following equation:

$$x = \frac{2b \sin|\beta - \gamma|}{d_1 + d_s}. \tag{3}$$

Here, b is the distance between the centres of the drops before the collision, β is the angle between the trajectory of the small drop and the centre-to-centre line, and γ is the angle between the trajectory of the small drop and the relative velocity vector, which is calculated from the following relation:

$$\gamma = \sin^{-1}\left(\frac{u_1}{u}\sin\alpha\right). \tag{4}$$

More than five hours of video tape from different collision outcomes are closely studied. A selected number of data points for different types of collisions and their boundaries are obtained for a range of Weber numbers and impact parameters, and for three different size ratios $\Delta = 0.5$, 0.75, and 1. A series of colour photographs aids our description of binary drop collision.

3.1. *Collision of two equal-size drops, $\Delta = 1$*

Figure 2 shows the regions for different types of collision outcomes for two equal-size drops in the Weber-number range of $5 \leqslant We \leqslant 100$, and all impact parameters, $0 \leqslant x \leqslant 1$. For this Weber-number range three collision outcomes, namely coalescence, reflexive separation and stretching separation are identified. These collision outcomes are described next.

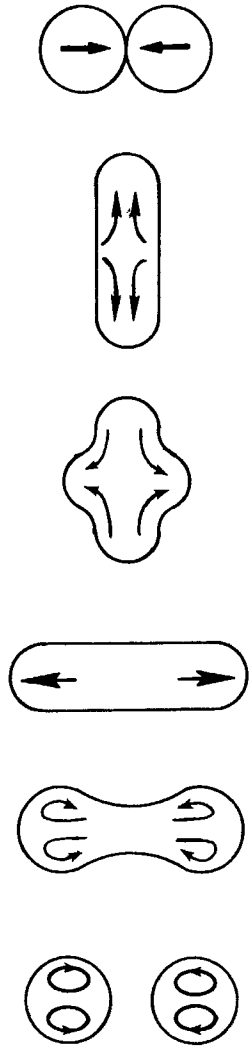

FIGURE 3. Schematic of reflexive separation for the head-on collision of two equal-size drops.

3.1.1. *Reflexive separation collision*

This refers to the outcome of collisions with impact parameters below the limit set by the lower curve in figure 2. The easiest way of describing reflexive separation is by considering the head-on collision of two equal-size drops as shown schematically in figure 3. Head-on collision refers to collisions in which the relative velocity vector coincides with the centre-to-centre line (i.e. $x = 0$). When two equal-size drops collide head-on they form a disk-like or a torus-like drop, the exact shape of which depends on the Weber number. A top view of a torus-like drop is shown in figure 4. It is called a torus-like, because it does not have a hole at the centre, instead a thin liquid film is always observed. Owing to the large curvature at the circumference of this disk-/torus-like drop, there will be a pressure difference between its inner and outer regions. The disk will therefore contract radially inward, and will push the liquid out from its centre. The contraction process is therefore a reflexive action by the liquid surface. This reflexive action will eventually generate a long cylinder with rounded

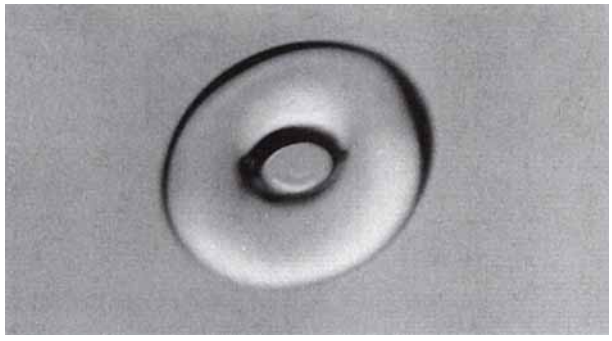

FIGURE 4. Top view of a head-on collision of two equal-size drops.

ends (figure 3). If the initial Weber number is not large, this cylinder will just oscillate until a spherical drop is formed. However, as the Weber number is increased, a critical condition will be reached, at which point the liquid cylinder formed after the surface reflex, will break into two drops. This critical point is the onset of the type of collision outcome which we call *reflexive separation*, as it is the reflexive action of the surface-tension forces that causes the separation.

The experimental results show that, for equal-size drops, the onset of reflexive separation is at $We = 19$, and $x = 0$. At this point two drops are generated with no satellites. (The Satellite drop is a relative term used to identify drops whose diameters are much smaller than the other surrounding drops.) The drops essentially keep their identities with little mass transfer during the formation of disk-/torus-like drops and the cylinder extending periods. Figure 5 (plate 1) shows a reflexive separation of two water drops with no satellites at $We = 23$ and $x = 0.05$. One of the streams is coloured to show the extent of mass transfer during the reflexive separation. Because the impact parameter is not exactly equal to zero, figure 5 shows a small amount of mass transfer between the two drops.

During a head-on collision, as the Weber number is increased the reflexive separation becomes more complicated. This is due to the generation of a thinner disk/torus and, consequently, formation of a longer cylinder. As the Weber number is increased, first a satellite is generated in the middle of the two bigger drops which are called the primary drops. The satellite size grows with increase in Weber number. At $We = 44$ the satellite size becomes equal to those of the primary drops. Figure 6 (plate 1) shows three-drop reflexive separation at $We = 40$ and $x = 0$. The centre drop usually goes through large oscillations before it becomes spherical. It should also be noted that the mass of the centre drop is a mixture of the masses of the two parent drops. If the Weber number is further increased, the size of the middle drop becomes bigger than those of primary drops.

At higher Weber numbers the liquid cylinder formed after the surface reflex becomes so long that it breaks into four drops. The number of drops formed increases with increase in Weber number. For instance, four-drop reflexive separation is observed at $We = 83$, five drops at $We = 96$, seven drops at $We = 103$, nine drops at $We = 146$, ten drops at $We = 154$, and thirteen drops at $We = 184$. Figure 7 (plate 1) shows a five-drop reflexive separation at $We = 96$ for a slightly off-centre collision. It should be noted that the edge drops break off first.

Effect of impact parameter. Reflexive separation is also observed for impact parameters other than zero. However, as the impact parameter is increased, the reflexive separation becomes more complicated. If the collision is not head-on (i.e.

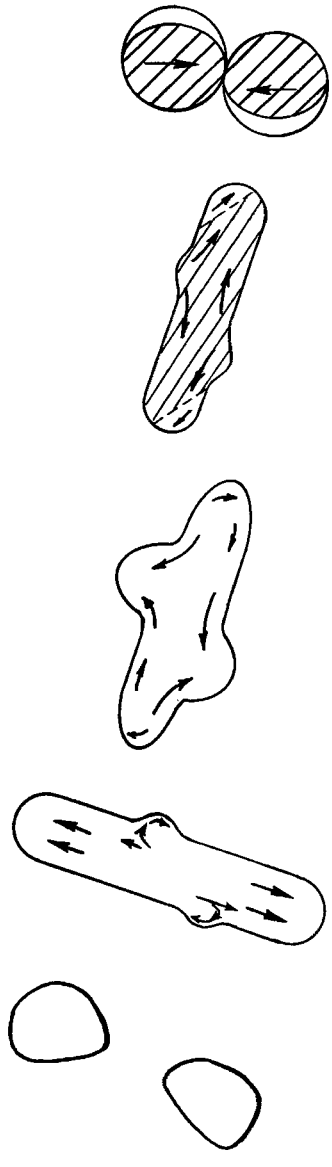

FIGURE 8. Schematic of reflexive separation for the off-centre collision of two equal-size drops.

off-centre collision) only part of the collision energy goes to the reflex action, and the rest will tend to stretch the combined mass in the directions of their initial trajectories. (Here, the combined mass is defined as the total liquid mass of the two collided drops prior to the final outcome of the collision.) These competing effects will generate a four-lobed-shaped drop. A schematic of an off-centre reflexive collision is shown in figure 8. Comparing figure 8 with the head-on collision of figure 3, one can see large differences in the shapes of the combined mass. The reflexive separation is easier if the shape of the combined mass shortly after the collision is smooth. This usually happens for smaller impact parameters: for instance, a head-on collision usually results in smooth disk-/torus-like drops (see figure 4). The contraction of such a drop unifies the internal fluid flow which is mainly moving in two opposite

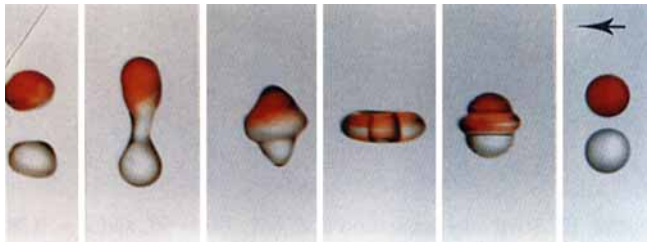

FIGURE 5. Reflexive separation with no satellite for $\Delta = 1$, $We = 23$, and $x = 0.05$.

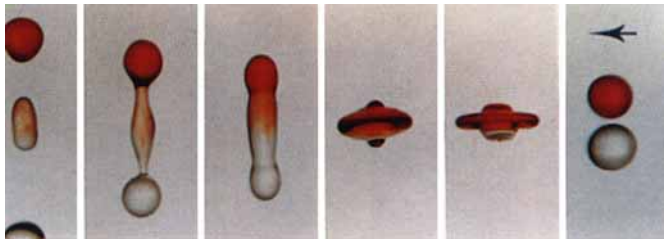

FIGURE 6. Three-drop reflexive separation for $\Delta = 1$, $We = 40$, and $x = 0$.

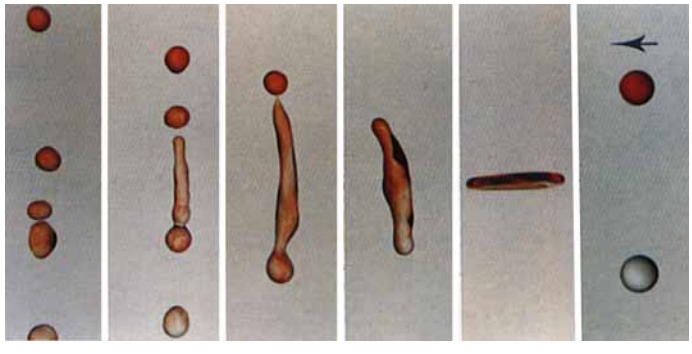

FIGURE 7. Five-drop reflexive separation for $\Delta = 1$, $We = 96$, and $x \sim 0$.

FIGURE 10. Off-centre reflexive separation for $\Delta = 1$, $We = 40$, and $x = 0.1$. The formation of a four-lobed drop after the collision is shown.

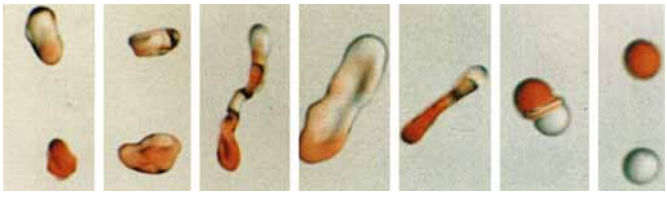

FIGURE 12. Stretching separation at $\Delta = 1$, $We = 53$, and $x = 0.38$.

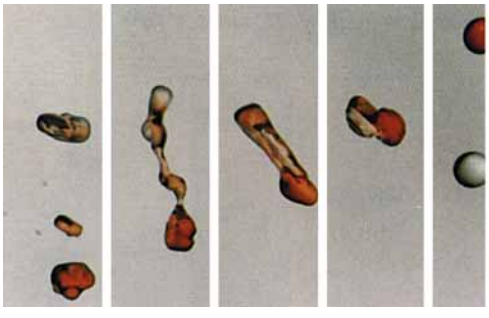

FIGURE 13. One-satellite stretching separation at $\Delta = 1$, $We = 83$, and $x = 0.34$.

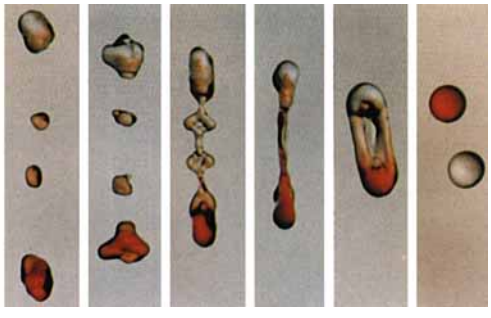

FIGURE 14. Stretching separation at $\Delta = 1$, $We = 83$, and $x = 0.43$.

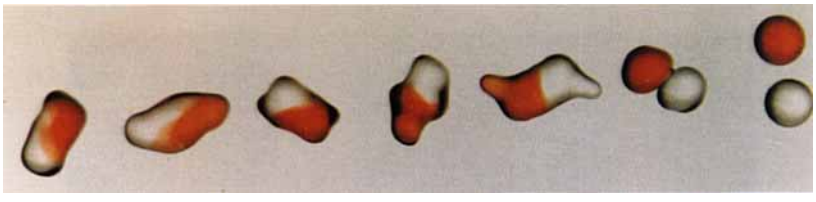

FIGURE 15. Coalescence collision at $\Delta = 1$, $We = 10$, and $x = 0.5$.

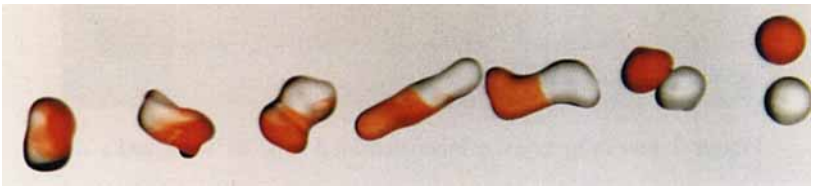

FIGURE 16. Coalescence collision at $\Delta = 1$, $We = 10$, and $x = 0.7$.

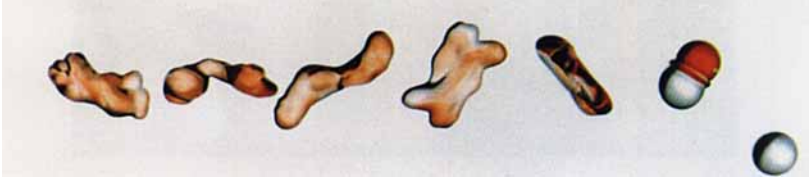

FIGURE 17. Coalescence collision at $\Delta = 1$, $We = 53$, and $x = 0.28$.

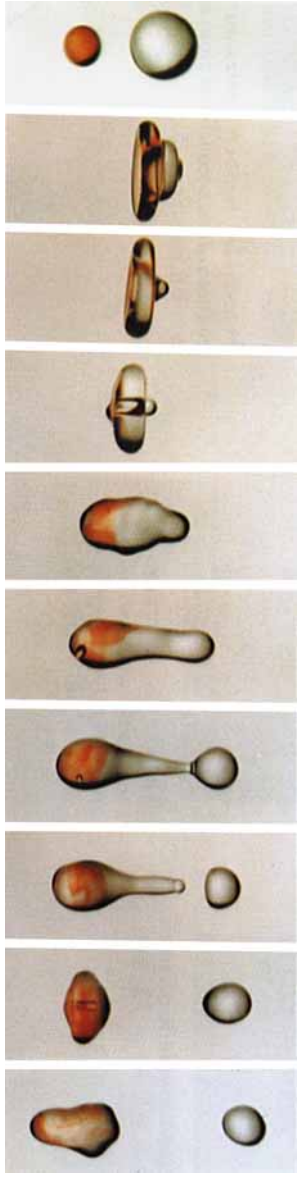

FIGURE 20. Reflexive separation collision of two unequal-size drops at $\Delta = 0.5$, $We = 56$, and $x = 0$.

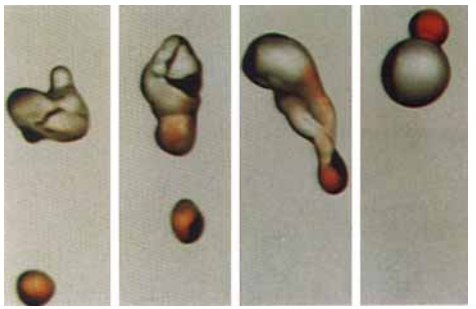

FIGURE 21. Stretching separation collision of two unequal-size drops at $\Delta = 0.5$, $We = 52$, and $x = 0.4$.

FIGURE 22. Stretching separation collision of two unequal-size drops at $\Delta = 0.47$, $We = 139$, and $x = 0.5$.

FIGURE 23. Head-on coalescence collision of two unequal-size drops at $\Delta = 0.6$, and $We = 25$.

FIGURE 24. Air entrapment during the coalescence collision of two unequal-size drops at $\Delta = 0.65$, $We = 30$, and $x = 0.05$.

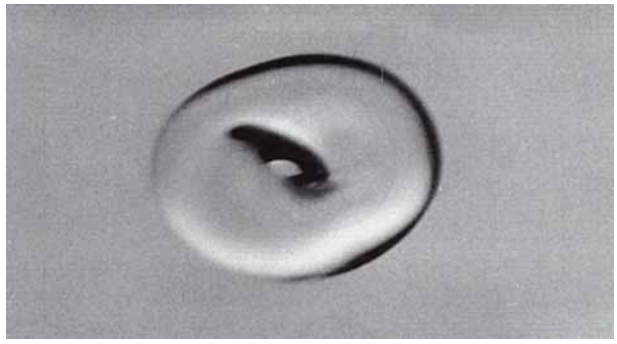

FIGURE 9. Top view of a slightly off-centre collision of two equal-size drops.

directions. This opposing flow condition will favour reflexive separation. For an off-centre collision a deformed disk-/torus-like drop is formed (a top view of one is shown in figure 9). The contraction of this deformed drop produces a mixed internal flow which reduces the effective reflexive action. Figure 10 (plate 1) shows a reflexive separation at $We = 40$ and $x = 0.1$. The four-lobed-shaped drop that appears after the reflexive action is clearly seen. Also, the distribution of the red colour in the combined mass shows the existence of large amounts of mass transfer. In figure 10 only two drops are generated after the collision, indicating that the reflex action is smaller than for the collision in figure 6 where three drops were formed for the same Weber number.

The experimental results show that as the impact parameter is increased, the total number of drops produced by the reflexive action reduces. For example, at the onset of reflexive separation, $We = 19$, an off-centre collision results in coalescence. Also, if the head-on collision produces three equal-size drops, an increase in the impact parameter will lead to the reduction of the size of the middle drop, and eventually only two drops are formed. If the head-on collision produces five drops, the increase in the impact parameter will make the collision outcome go through four, three, two drops, and finally coalescence.

3.1.2. *Stretching separation*

When two drops collide at high impact parameters, only a portion of them will come in direct contact, resulting in a region of interaction. This region of interaction is shown in figure 11 as the cross-hatched section. The remaining portions of the drops will tend to flow in the direction of their initial trajectory and consequently stretch the region of interaction. Therefore, the outcome of collision will depend on the competition between the surface energy of the region of interaction, which is trying to hold the two drops together, and the portion of the initial drop kinetic energy which is trying to stretch and separate the combined mass. For the same Weber number if the impact parameter increases, the region of interaction reduces, resulting in a higher ratio of stretching energy over the surface energy of the interaction region. Separation occurs when this ratio reaches a critical value, which will be quantified in §4.3. We refer to this kind of separation as stretching separation.

The boundary between coalescence and stretching separation is shown by the upper curve in figure 2. At the onset of separation, for any Weber number, two drops of similar size, without any satellite, will be produced. The increase of impact parameter will result in the generation of one satellite between the two drops. As the impact parameter increases the number of satellites increases until a critical impact

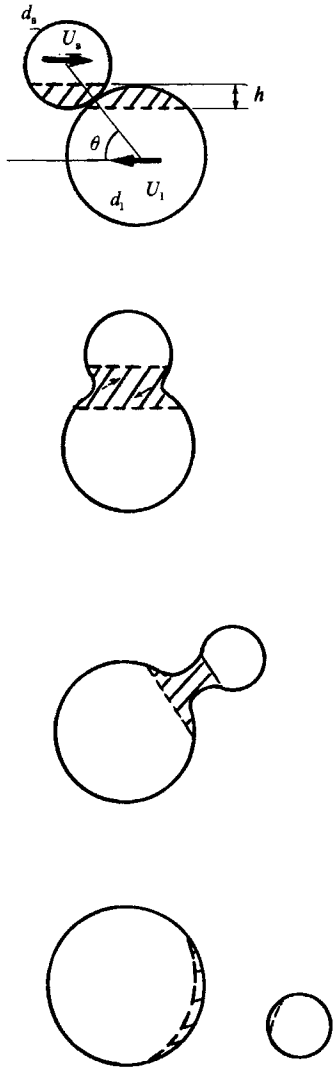

FIGURE 11. Schematic of the stretching separation collision of two drops.

parameter is reached. Further increase in the impact parameter will reduce the number of satellites. One interesting feature of stretching separation is that the size of the satellites below this critical impact parameter are larger than the satellite sizes above it. The maximum number of satellites generated is related to the Weber number.

Figure 12 (plate 2) shows a stretching separation for $We = 53$ and $x = 0.38$, which results in only two drops. After separation the two drops are severely deformed, and show some degree of mass transfer. Figures 13 and 14 (plate 2) show one-satellite and two-satellite stretching separations at $We = 83$ and for $x = 0.34$ and $x = 0.43$ respectively. Figure 14 clearly shows the stretching of the region of interaction, which eventually under the action of surface tension will contract and form two satellite drops. At higher impact parameters, more satellites will be formed.

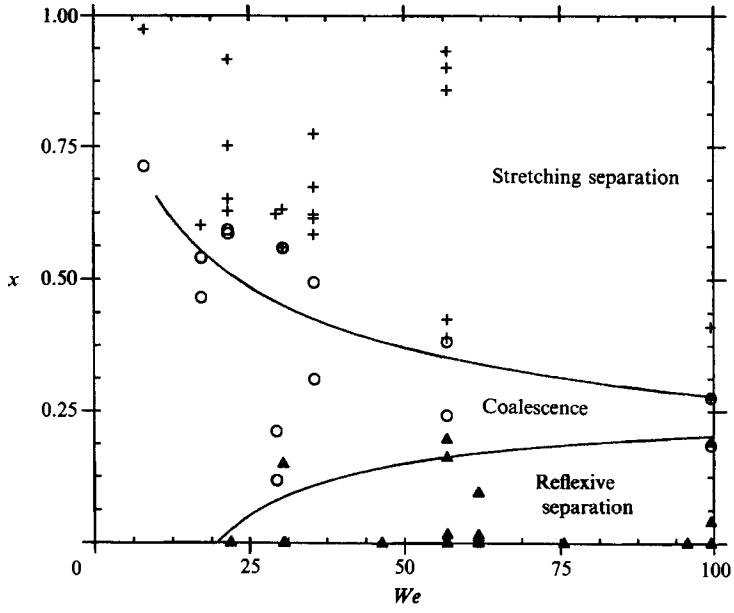

FIGURE 18. Analytically obtained regions of coalescence, reflexive separation, and stretching separation for drop size ratio $\Delta = 0.75$, together with experimental data (symbols as figure 2).

3.1.3. *Coalescence*

The experimentally obtained coalescence region is shown in figure 2. At Weber numbers between 1 and 19 and for small impact parameters, all collisions result in coalescence. (Recall that the boundaries between coalescence and bouncing collisions are not reported here.) Figures 15 and 16 (plate 2) show coalescence collisions at $We = 10$. The evolutionary process in a coalescence collision at low Weber numbers is governed by the competition between stretching and drop drainage. Drop drainage refers to the flow of liquid from the higher pressure drop region into the point of contact to form a liquid bridge. The higher the impact parameter the higher the stretching and, therefore, the shorter the time for drainage. It is seen that as the impact parameter increases less mass moves towards the bridge zone, as is evident by comparing figures 15 and 16. Figure 17 (plate 2) shows a coalescence collision at $We = 53$ and $x = 0.28$. For higher-Weber-number collisions, the coalesced drop is more deformed and the mass transfer is faster.

3.2. *Collision of two drops of different sizes*

The collision dynamics of two drops with size ratios of 0.75, and 0.5 are also investigated. The results are presented in figures 18 and 19. These figures show that as the size ratio decreases both the reflexive and stretching separation regions become smaller. Hence, the coalescence region becomes larger. The collision phenomena for these cases are described next.

3.2.1. *Reflexive separation*

For two drops of different diameters, the phenomenon is generally more complex. A photograph of the reflexive separation at $\Delta = 0.5$, $We = 56$, and for close to head-on collision is shown in figure 20 (plate 3). Similarly to other head-on collisions, the liquid in both drops will spread radially in the plane normal to the centre-to-centre line. This will generate a disk-like drop which will later contract, forming a liquid

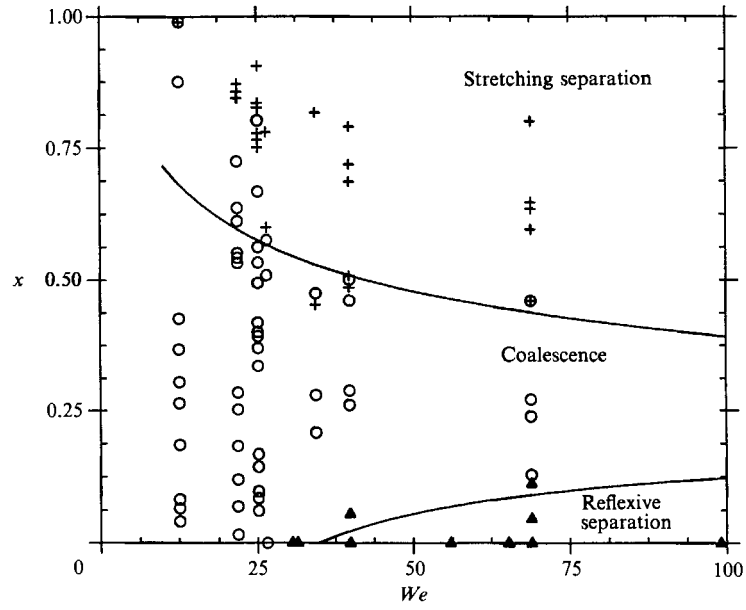

FIGURE 19. Analytically obtained regions of coalescence, reflexive separation, and stretching separation for drop size ratio $\Delta = 0.5$, together with experimental data (symbols as figure 2).

column. Unlike the liquid column formed by the collision of equal-size drops, drops with different sizes form an asymmetric column. For high enough Weber numbers, this column will eventually break into two or more drops. For instance, for the head-on collision of two drops with $\Delta = 0.8$, at $We = 30$, two drops are formed, at $We = 56$ three drops, and at $We = 75$ five drops.

A very interesting feature of reflexive separation of two drops with different sizes is that the initially large drop becomes smaller after the collision and vice versa: the initially small drop takes some mass from the large drop, during the contact time, and becomes larger after the collision. As the impact parameter increases, it becomes more difficult to obtain reflexive separation. It is observed that off-centre collisions result in shorter columns which may also be curved. These columns usually break into a fewer number of drops than for a head-on collision. A more detailed description of the phenomena is given by Poo (1989).

3.2.2. *Stretching separation*

As was described earlier, the separation phenomenon is characterized by the stretching of the region of interaction, or the bridge zone. At a given Weber number stretching separation happens at higher impact parameters for smaller diameter ratio collisions. The reason is that the momentum of the smaller drop cannot overcome the inertia and the surface forces in the region of interaction. The collision outcome of two unequal-size drops is governed by two opposing effects, namely drop drainage and drop stretching. Because of the size ratio, there would be a pressure difference between the two drops, the smaller drop being at higher pressure. Therefore, as soon as the bridge is formed liquid will tend to flow from the small drop to the large drop. The total mass transfer will depend on the contact time of the two drops, which in turn is dependent on the Weber number. Therefore, as the contact time shortens, the drainage effect will reduce, resulting in smaller mass transfer from the small drop to the large drop. On the other hand, at a given impact parameter as

the Weber number increases, the stretching effect will increase. Because the large drop appears softer to the small drop, the small drop will scoop up some of its mass. Therefore, the stretching effect for unequal-size drops will cause mass transfer from the large drop to the small drop. The two opposing effects of drainage and stretching will determine the size of the drops after the collision. Figure 21 (plate 4) ($\Delta = 0.5$, $We = 52$, $x = 0.4$) clearly shows the drainage effect during the contact time. Figure 22 (plate 4) shows stretching separation for $\Delta = 0.47$ at a high Weber number of 139 and $x = 0.5$. As the Weber number increases, the smaller drop tends to shear off more of the mass of the large drop and generates more satellites.

3.2.3. *Coalescence*

Generally, it is more difficult for two unequal-size drops to separate after the collision than for two equal-size drops. This is because in the former case the mass in the small drop during the collision will tend to flow into the large drop. Figure 23 (plate 4) shows a head-on coalescence collision for $\Delta = 0.6$ and $We = 25$. For this Weber number, the reflexive action is not strong enough to break the drops, as it was observed in figure 20. Therefore, the combined mass simply oscillates until a spherical drop is formed. It should be noted that, similarly to most low-Weber-number collisions, there is very little mixing during the initial period of the collision. In figure 24 (plate 4) a collision at $We = 30$ and $\Delta = 0.65$ is shown. The small drop forms a large cavity in the large drop. In the process of contraction an air bubble gets trapped in the drop. This is exclusively observed in unequal-size drop collision.

4. Theoretical prediction of reflexive and stretching separation

A detailed theoretical treatment of the collision dynamics of liquid drops requires the solution of the unsteady three-dimensional Navier–Stokes equations with free surfaces. Numerical simulation of drop collision is presently being carried out by these authors and its results will be published in the near future. However, the occurrence of different types of collisions can be predicted by a simple energy balance analysis. In this type of analysis one has to develop a physical criterion to explain the occurrence of a particular collision type, based on which a simple parametric relationship can be found to define the boundaries of that collision type. In the following sections we shall present criteria for the occurrence of reflexive and stretching separation, respectively.

4.1. *Effective reflexive energy*

In this section we shall introduce the concept of effective reflexive energy, which is assumed to be the cause of the reflexive separation. Consider the collision of a pair of drops using mass-centre coordinates, as shown in figure 3. In this coordinate system, the drops after the collision will be in a state of combined mass, which has no translational kinetic energy. Therefore, the total energy of the combined mass at any state will only comprise the surface energy, and the internal kinetic energy. The dissipated energy for a water drop is not significant and it is neglected. This can be justified by calculating the Laplace number $Lp(=We/Re^2)$ which indicates the ratio of the viscous effects to the surface tension effects. For viscous dissipation to be important the Laplace number has to be large. However, in the range of parameters studied here, Lp is small, of the order of 10^{-4}. We shall assume that the combined mass at any phase of the collision process can be transformed into a nominal spherical drop which has the same volume as the sum of the volumes of the parent

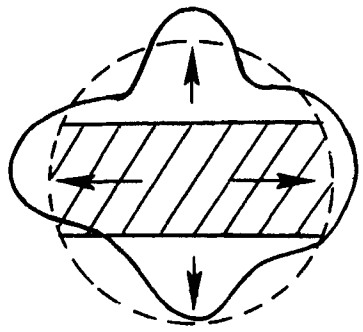

FIGURE 25. The nominal spherical drop which represents the energy state of the combined mass throughout the collision process.

drops (figure 25). The internal kinetic energy of this nominal drop, K_n, is then equal to the sum of the kinetic and surface energies of the parent drops minus the surface energy of the nominal drop.

If the nominal drop is going to undergo reflexive separation, there must be some opposing flows inside the drop. We shall call these flows reflexive flows. Based on the experimental observations it is evident that the reflexive flows are generated by the surface reflex. In the collision of two liquid drops the reflexive action is generated by two effects. The first effect is due to the flows in the portions of drops before collision which directly oppose each other. We shall refer to these flows as the counteractive flows. Figure 8 shows the counteractive flow region by the cross-hatched lines. The second source of reflexive action is due to the surface-induced flows. This is easily understood by referring to figure 3 and assuming that the drops are not moving. When two drops with zero initial velocities are brought into contact, the surface tension effects will force the flow towards the contact point. This phenomenon, which we previously called the drainage effect, after the reflexive action will generate opposing flows in the combined mass. We shall refer to these flows as the excess surface-induced flows, since they are generated by the excess surface energy (the difference between the surface energy of the parent drops and that of the nominal spherical drop).

The kinetic energy of the counteractive flows, K_c, is generated by the portions of drops which directly oppose each other. These portions are assumed to be the prolate regions in each drop with their axes passing through the middle of the impact parameter (figure 8). Therefore, K_c is equal to

$$K_c = \tfrac{1}{2}\rho(V_{lp}\, U_l^2 + V_{sp}\, U_s^2), \tag{5}$$

where V_{sp} and V_{lp} are the volumes of the prolate regions in the small and large drops respectively, given by

$$V_{sp} = \tfrac{1}{6}\pi d_l^3(\Delta-\xi)^2(\Delta^2-\xi^2)^{\frac{1}{2}} \tag{6}$$

and

$$V_{lp} = \tfrac{1}{6}\pi d_l^3(1-\xi)^2(1-\xi^2)^{\frac{1}{2}}, \tag{7}$$

where

$$\xi = \tfrac{1}{2}x(1+\Delta). \tag{8}$$

U_l and U_s are the velocities of the large and small drops in the mass-centre coordinates respectively, given by

$$U_l = \frac{\Delta^3 u}{1+\Delta^3}, \tag{9}$$

$$U_s = \frac{u}{1+\Delta^3}. \tag{10}$$

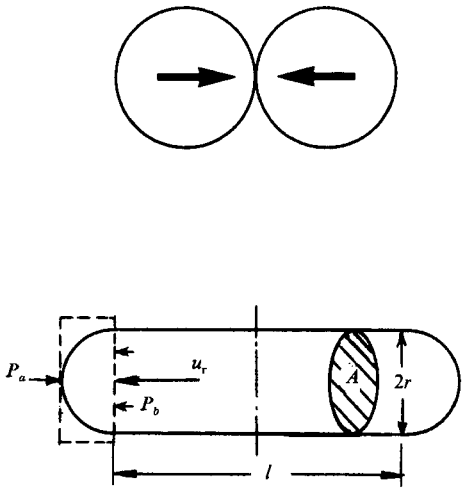

FIGURE 26. A description of the drop internal flow velocity for the onset of reflexive separation.

The kinetic energy of the excess-surface-induced flows, K_e, is equal to the difference between the surface energy of the parent drops and that of the combined mass. That is

$$K_e = \sigma\pi d_1^2[(1+\Delta^2)-(1+\Delta^3)^{\frac{2}{3}}]. \tag{11}$$

Up to this point we have only considered the opposing flows due to the reflex actions. However, for off-centre collisions, as discussed in §3, part of the initial drop kinetic energy will try to stretch the combined mass. The stretch-generated flows, called the stretching flows, are approximately perpendicular to the reflexive flows (see figures 8 and 25). The stretching flows reduce the reflexive energy. The kinetic energy of the stretching flows is basically equal to the leftover kinetic energy of the parent drops. That is

$$K_s = \tfrac{1}{2}\rho[(V_l - V_{lp})\,U_l^2 + (V_s - V_{sp})\,U_s^2], \tag{12}$$

where V_l and V_s are the total volumes of the large and small drops, respectively. Based on the above discussions, the effective reflexive energy, K_r, can then be calculated from the following equation:

$$K_r = K_e + K_c - K_s \tag{13}$$

or

$$K_r = \sigma\pi d_1^2\left[(1+\Delta^2)-(1+\Delta^3)^{\frac{2}{3}} + \frac{We}{12\Delta(1+\Delta^3)^2}(\Delta^6\eta_1+\eta_2)\right], \tag{14}$$

where

$$\eta_1 = 2(1-\xi)^2(1-\xi^2)^{\frac{1}{2}} - 1, \tag{15}$$

$$\eta_2 = 2(\Delta-\xi)^2(\Delta^2-\xi^2)^{\frac{1}{2}} - \Delta^3. \tag{16}$$

4.2. *Reflexive separation criterion*

We shall now present a criterion for the occurrence of reflexive separation, using the simplest case of the collision of two equal-size drops for the development of our model. When the two drops collide, they first form a thin disk which will later contract into a slender cylinder. As the reflexive energy stretches the spherical drop, a round-ended cylinder with radius r and length $l+2r$, is formed (figure 26). Based on Rayleigh's (1945) linear theory, if the length-to-diameter ratio of a liquid column is equal to π, the column becomes unstable. The round-ended cylinder is, however, different from a liquid column, which does not have surface forces pushing in from

its two ends. For this drop with $l/r = 2\pi - 2$, if the fluid inside is stagnant, the surface forces from the two ends will force the flow towards the centre, preventing the breakup. The liquid cylinder can break only if the internal flow field stops the retraction of the two ends. In this manner, the round-ended cylindrical drop is held in space and time, and the disturbances can grow and break the drop. An estimation of the internal velocity that is just enough to sustain this drop shape is now attempted.

Take a control volume at the left-hand end of the cylinder, as shown in figure 26. The force balance can be written as

$$\frac{\mathrm{d}}{\mathrm{d}t}\int u'\rho\,\mathrm{d}V - \rho u_{\mathrm{r}}^2 A = (p_b - p_a)A, \tag{17}$$

where $p_a = 2\sigma/r$, p_b is estimated as σ/r, u_{r} is the reflexive velocity, A is the cross-sectional area, and V is the volume. The unsteady term can be estimated as $\bar{u}'\,\mathrm{d}m/\mathrm{d}t$, where the average velocity, $\bar{u}'$, is approximated by $\frac{1}{2}u_{\mathrm{r}}$. Also, the term $\mathrm{d}m/\mathrm{d}t$ is just $\rho u_{\mathrm{r}}^2 A$. With all the terms estimated, the velocity u_{r} can be solved to be

$$u_{\mathrm{r}} = \left(\frac{2\sigma}{\rho r}\right)^{\frac{1}{2}}. \tag{18}$$

The velocity distribution within the cylinder is not readily determined. However, owing to the ease of flow of the liquid in the drop, it is appropriate to say that, except in the vicinity of the centreplane, the above-calculated velocity magnitude should exist in most of the cylinder. Therefore, the minimum kinetic energy within the drop that is needed to sustain its shape, can be approximated as follows:

$$K_{\mathrm{m}} = 4\pi r^2\sigma\left[\frac{1}{3} + \frac{1}{4}\frac{l}{r}\right]. \tag{19}$$

The round-ended cylindrical drop is now transformed into a nominal spherical drop. The reflexive kinetic energy and the surface energy of this drop will then represent the critical conditions for the onset of reflexive separation. The reflexive kinetic energy of this nominal spherical drop, K_{r}^*, is therefore equal to

$$K_{\mathrm{r}}^* = K_{\mathrm{m}} + S_{\mathrm{m}} - S_{\mathrm{n}}^*, \tag{20}$$

where K_{m} is defined by (19), S_{m} is the surface energy of the round-ended cylindrical drop, and S_{n}^* is the surface energy of the critical nominal spherical drop (i.e. $S_n^* = 4\pi r^2\sigma(1 + 3l/4r)^{\frac{2}{3}}$). The ratio of the reflexive kinetic energy to the surface energy of the critical nominal drop, Γ, will then represent a critical condition for the reflexive separation. This ratio is equal to

$$\Gamma = \frac{K_r^*}{S_{\mathrm{n}}^*} = \left(1 + \frac{3l}{4r}\right)^{-\frac{2}{3}}\left(\frac{4}{3} + \frac{3l}{4r}\right) - 1. \tag{21}$$

When $l/r = 2\pi - 2$, Γ is equal to 0.7425. According to the experimental results, for two drops of the same size colliding head on, the onset of reflexive separation occurs at $We = 19$. Based on this Weber number the critical kinetic energy for reflexive separation can be obtained. The reflexive kinetic energy is equal to the critical kinetic energy calculated this way plus the excess surface energy given in (11). The reflexive kinetic energy calculated this way is about 0.73 of the nominal surface energy. The above calculation of Γ is therefore verified by the experiment.

Based on our definition of reflexive kinetic energy, K_r^*, which is the cause of separation, and the surface energy of the nominal spherical drop, S_n^*, which prevents the separation, one might expect that separation should occur when $K_r^* \geqslant S_n^*$. However, it should be noted that the breakup process of the nominal spherical drop is a transient one in which the drop shape changes continuously. Therefore when, for instance, the drop shape takes the form shown in figure 3 at the fifth stage, the surface energy of the neck region will actually help the separation rather than preventing it. It is, therefore, not surprising to see that the reflexive energy does not have to be as large as the nominal spherical drop surface energy for separation to occur.

We now postulate that *for a nominal spherical combined mass, when the effective reflexive kinetic energy is more than 75% of its nominal surface energy, reflexive separation will occur.* That is, the criterion for reflexive separation is

$$K_r \geqslant 0.75\sigma\pi(d_1^3+d_s^3)^{\frac{2}{3}}. \tag{22}$$

To find the boundary between coalescence and reflexive separation, we take the equal sign and use (14) for K_r to derive the following equation:

$$\frac{We}{\Delta(1+\Delta^3)^2}(\Delta^6\eta_1+\eta_2)+3[4(1+\Delta^2)-7(1+\Delta^3)^{\frac{2}{3}}] = 0. \tag{23}$$

4.3. *Stretching separation*

Consider collision of a pair of drops at a high impact parameter as shown in figure 11. As it was discussed in §3.1.2 only a small portion of the drops will come into contact, resulting in a region of interaction. The remaining portions will tend to move in the direction of their initial trajectory. The stretching separation energy therefore consists of two parts. One is the kinetic energy of the region of interaction, and the other is the remaining part of the total kinetic energy. The effective kinetic energy of the region of the interaction is obtained by using the component of the drop velocities in the separating direction of the drops as shown in figure 11.

In stretching separation the region of interaction is the portions of the drops which overlap each other. The width of the overlapping region is simply equal to the sum of the drop radii minus the impact parameter, i.e. $h = \frac{1}{2}(d_1+d_s)(1-x)$. The volumes of the interacting regions are found from the following equations:

$$V_{si} = \phi_s V_s, \tag{24}$$

$$V_{li} = \phi_l V_l, \tag{25}$$

where ϕ_s and ϕ_l are defined as follows:

$$\phi_s = \begin{cases} 1-\dfrac{1}{4\Delta^3}(2\Delta-\tau)^2(\Delta+\tau) & \text{for } h > \frac{1}{2}d_s \\ \dfrac{\tau^2}{4\Delta^3}(3\Delta-\tau) & \text{for } h < \frac{1}{2}d_s \end{cases} \tag{26}$$

and

$$\phi_l = \begin{cases} 1-\frac{1}{4}(2-\tau)^2(1+\tau) & \text{for } h > \frac{1}{2}d_l \\ \dfrac{\tau^2}{4}(3-\tau) & \text{for } h < \frac{1}{2}d_l \end{cases} \tag{27}$$

where $\tau \equiv (1-x)(1+\Delta)$.

The total effective stretching kinetic energy is therefore equal to

$$K_{si} = \tfrac{1}{2}\rho[(V_s - V_{si})\,U_s^2 + (V_l - V_{li})\,U_l^2] + \tfrac{1}{2}\rho[V_{si}(U_s \sin\theta)^3 + V_{li}(U_l \sin\theta)^2], \tag{28}$$

where θ is the angle between the relative velocity vector and the centre-to-centre line at the time of collision (see figure 11). Therefore, $\sin\theta = x$. Note that the terms in the first square bracket on the right-hand side of (28) represent the kinetic energy of the region outside of the region of interaction, and the terms in the second square bracket are the effective stretching kinetic energies of the region of interaction. Equation (28) can be written in the following form:

$$K_{si} = \tfrac{1}{2}\rho U^2 V_l^2 \left\{\frac{\Delta^3}{(1+\Delta^3)^2}[(1+\Delta^3) - (1-x^2)(\phi_s + \Delta^3\phi_l)]\right\}. \tag{29}$$

The surface energy at the region of interaction is assumed to act against the stretching kinetic energy. The surface energy associated with the region of interaction is estimated as the surface energy associated with a cylinder with the same volume and with height h. (Another cylinder with the same volume but with diameter equal to the diameter of the smaller drop was also considered. However, the results were not as good.) The surface energy of the region of interaction is therefore equal to

$$S_{si} = 2\sigma[\pi h(V_{si} + V_{li})]^{\frac{1}{2}}$$

or

$$S_{si} = \sigma[2\pi V_l d_l \tau(\Delta^3\phi_s + \phi_l)]^{\frac{1}{2}}. \tag{30}$$

The criterion for stretching separation is assumed to be when the total effective stretching kinetic energy, K_{si}, is larger than the surface energy of the region of interaction, which is opposing the separation. That is

$$K_{si} \geqslant S_{si}. \tag{31}$$

Using the equal sign the stretching separation boundary can be calculated from the following equation:

$$We = \frac{4(1+\Delta^3)^2[3(1+\Delta)(1-x)(\Delta^3\phi_s + \phi_l)]^{\frac{1}{2}}}{\Delta^2[(1+\Delta^3) - (1-x^2)(\phi_s + \Delta^3\phi_l)]}. \tag{32}$$

5. Comparison with experimental data and other theories

The theoretically derived curves for reflexive and stretching separation collisions are plotted as solid lines in figures 2, 18, 19, along with the experimental data. The theoretical prediction of the boundaries between different types of collision is good. As there has been no previous theoretical prediction for the boundary between the reflexive separation and coalescence collision, only the model presented here, (23), is plotted in figures 2, 18, 19. However, there are other theoretical predictions for the stretching separation collision, which can be compared to our model.

Three different theoretical treatments of the stretching separation phenomenon have been reported: Park (1970), Brazier-Smith *et al.* (1972) and Arkhipov *et al.* (1983). Park (1970) derived his equation from balancing the surface tension in the region of contact and the angular momentum. His equation in our notation can be written as

$$x = \left(\frac{12}{\pi}\right)^{\frac{1}{2}} \frac{(\Delta^2 - \Delta + 1)^{\frac{1}{2}}}{\Delta We^{\frac{1}{2}}} \left[\frac{(1+\Delta^5)(\Delta^2 - \Delta + 1)}{5\Delta^3} + \frac{(1+\Delta)}{2}\right]\left[4 - \left[x(1+\Delta) - \frac{(1-\Delta)}{x}\right]^2\right]^{\frac{1}{4}}. \tag{33}$$

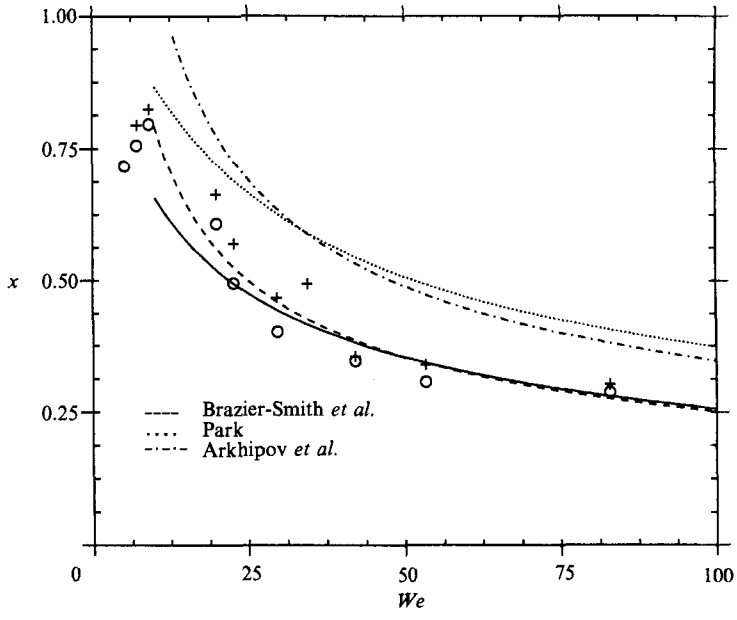

FIGURE 27. Comparison of different stretching separation theories with the experimental results for drop size ratio $\Delta = 1.0$.

Brazier-Smith *et al.* (1972) suggested that separation will occur if rotational energy exceeds the surface energy required to reform the two drops from a coalesced nominal drop. Based on this criterion, they obtained the following relation:

$$x = \left(\frac{24}{5We}\right)^{\frac{1}{2}} \frac{(1+\Delta^3)^{\frac{11}{6}}}{(1+\Delta)\,\Delta^{\frac{5}{2}}} [1+\Delta^2-(1+\Delta^3)^{\frac{2}{3}}]^{\frac{1}{2}}. \tag{34}$$

Arkhipov *et al.* (1983) used the minimum-potential-energy variational principle by equating to zero the first variation of the potential energy of the system in a coordinate system rotating with constant angular velocity. They obtained the following relation for the boundary between the stretching separation and coalescence:

$$x = \frac{1}{\Delta^3}\left(\frac{6(1+\Delta^3)}{We}\right)^{\frac{1}{2}}. \tag{35}$$

These three curves are plotted in figures 27–29 for different size ratios. The results show that there is a significant difference between the three theories for different size ratios. The comparison with the experimental results shows that only the model presented here, (32), and Brazier-Smith *et al.*'s model, (34), can adequately predict the stretching separation boundary. However, for a small size ratio of $\Delta = 0.5$ even the Brazier-Smith *et al.* model does not provide a good prediction for the stretching separation boundary.

One important note regarding the previous models for stretching separation is that all the previous theories are based on a comparison between the rotational energy and some effective surface energy. They all assume that the angular momentum is the cause of the separation. However, a close look at the experimental results clearly indicates that stretching separation occurs much earlier than the development of any significant rotation. This stretching, as described before, is due to the tendency of the

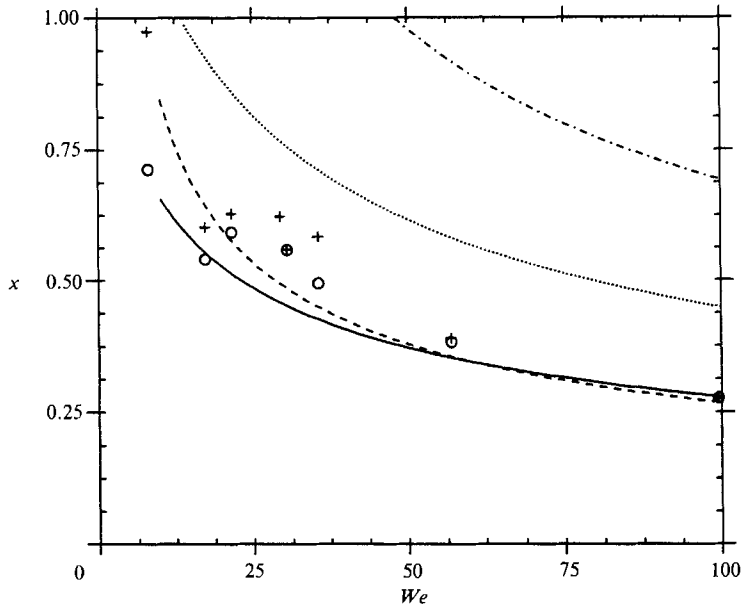

FIGURE 28. Comparison of different stretching separation theories with the experimental results for drop size ratio $\Delta = 0.75$. Curves defined in figure 27.

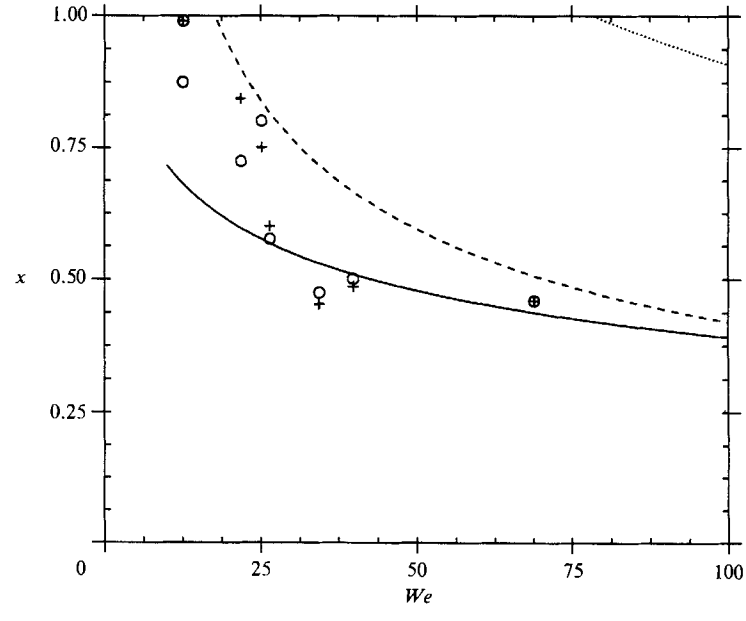

FIGURE 29. Comparison of different stretching separation theories with the experimental results for drop size ratio $\Delta = 0.5$. Curves defined in figure 27.

drops to move along their initial trajectory. Therefore, although some of the previous models, such as the one by Brazier-Smith *et al.*, predict the separation boundary closely, their criterion is not physically observed.

6. Concluding remarks

Binary-collision dynamics of two water drops in the Weber number range of 1 to 100 can be completely characterized based on the drop size ratio, the collision Weber number, and the impact parameter. In this Weber-number range, the Reynolds number does not seem to play a significant role in the outcome of a collision. Two fundamentally different separating collisions are observed. For close to head-on collisions, reflexive separation occurs. This is due to the reflexive action of the surface tension forces which results in two opposing flows internal to the combined mass. It is both experimentally and theoretically shown that the critical condition for the onset of reflexive separation occurs when the kinetic energy of these internal flows is larger than 75% of the surface energy of a nominal spherical drop having the same volume as the combined drops. Stretching separation on the other hand is simply due to the competition between the kinetic energy of the two drops and the surface energy of the region of interaction between them.

During reflexive separation the drops will follow a reflective type of trajectory; however, in stretching separation the drop trajectories after the separation deviate less. Reflexive separation may result in two or more drops. The number of drops formed depends on the Weber number, size ratio, and the impact parameter. For unequal-size-drop collisions, the small drop becomes larger and the size ratio of the drops in the string formed after separation reduces in the direction of the initially larger drop.

In reflexive separation the increase in the impact parameter will cause a reduction in the number of drops formed. In stretching separation the increase in the impact parameter will first increase the number of satellites formed until a critical impact parameter is reached. Further increase in the impact parameter will result in reduction of the number of satellites. During reflexive separation the mixing increases with increase in the impact parameter, the reverse happens during stretching separation.

REFERENCES

ADAM, J. R., LINDBLAD, N. R. & HENDRICKS, C. D. 1968 The collision, coalescence, and disruption of water droplets. *J. Appl. Phys.* **39**, 5173–5180.

ARKHIPOV, V. A., VASENIN, I. M. & TROFIMOV, V. F. 1983 Stability of colliding drops of ideal liquid. Tomsk. Translated from *Zh. Prikl. Mekh. Tekh. Fiz.* **3**, 95–98.

ASHGRIZ, N. & GIVI, P. 1987 Binary collision dynamics of fuel droplets. *Intl J. Heat Fluid Flow* **8**, 205–210.

ASHGRIZ, N. & GIVI, P. 1989 Coalescence efficiencies of fuel droplets in binary collisions. *Intl Commun. Heat Mass Transfer* **16**, 11–20.

BRADLEY, S. G. & STOW, C. D. 1978 Collisions between liquid drops. *Phil. Trans. R. Soc. Lond.* A **287**, 635–678.

BRADLEY, S. G. & STOW, C. D. 1979 On the production of satellite droplets during collisions between water drops falling in still air. *J. Atmos. Sci.* **36**, 494–500.

BRAZIER-SMITH, P. R., JENNINGS, S. G. & LATHAM, J. 1972 The interaction of falling water drops: coalescence. *Proc. R. Soc. Lond.* A **326**, 393–408.

COTTON, W. R. & GOKHALE, N. R. 1967 Collision, coalescence, and breakup of large water drops in a vertical wind tunnel. *J. Geophys. Res.* **72**, 4041–4049.

GORBACHEV, S. V. & MUSTEL, E. R. 1935 The lower stability limit of drops upon impact. *Kolloidzeitschrift* **73**, 20–24.

GORBACHEV, S. V. & NIKIFOROVA, V. M. 1935 The upper stability limit of drops upon impact. *Kolloidzeitschrift* **73**, 14–20.

JAYARATNE, O. W. & MASON, B. J. 1964 The coalescence and bouncing of water drops at an air/water interface. *Proc. R. Soc. Lond.* A **280**, 545–565.

JIANG, Y. J., UMEMURA, A. & LAW, C. K. 1990 An experimental investigation on the collision behaviour of hydrocarbon droplets. *J. Fluid Mech.* (submitted).

LEVIN, Z., NEIBURGER, M. & RODRIGUEZ, L. 1973 Experimental evaluation of collection and coalescence efficiencies of cloud drops. *J. Atmos. Sci.* **30**, 944–946.

LIST, R. & WHELPDALE, D. M. 1969 A preliminary investigation of factors affecting the coalescence of colliding water drops. *J. Atmos. Sci.* **26**, 305–308.

LOW, T. B. & LIST, R. 1982*a* Collision, coalescence and breakup of raindrops. Part I: Experimentally established coalescence efficiencies and fragment size distributions in breakup. *J. Atmos. Sci.* **39**, 1591–1606.

LOW, T. B. & LIST, R. 1982*b* Collision, coalescence and breakup of raindrops. Part II: Parameterization of fragment size distribution. *J. Atmos. Sci.* **39**, 1607–1618.

MCTAGGART, J. D. & LIST, R. 1975 Collision and breakup of water drops at terminal velocity. *J. Atmos. Sci.* **32**, 1401–1411.

O'ROURKE, P. J. & BRACCO, F. V. 1980 Modelling of drop interactions in thick sprays and a comparison with experiments. *Stratified Charged Auto Engng Conf.*, pp. 101–116. Inst. Mech. Engng.

PARK, J. Y. & BLAIR, L. M. 1975 The effect of coalescence on drop size distribution in an agitated liquid-liquid dispersion. *Chem. Engng Sci.* **30**, 1057–1064.

PARK, R. W. 1970 Behavior of water drops colliding in humid nitrogen. Ph.D. thesis, Department of Chemical Engineering, The University of Wisconsin, p. 577.

PODVYSOTSKY, A. M. & SHRAIBER, A. A. 1984 Coalescence and breakup of drops in two phase flows. *Intl J. Multiphase Flow* **10**, 195–209.

POO, J. Y. 1989 Experimental and numerical investigation of the binary drop collisions. Ph.D. thesis, Dept. Mech. and Aero. Eng., State University of New York at Buffalo.

RAYLEIGH, LORD 1945 *The Theory of Sound*, Vol. 2. Dover.

RYLEY, D. J. & BENNETT-COWELL, B. N. 1967 The collision behavior of steam-borne water drops. *Intl J. Mech. Sci.* **9**, 817–833.

SCHOTLAND, R. M. 1960 Experimental results relating to the coalescence of water drops with water surfaces. *Discuss. Faraday Soc.* **30**, 72–77.

SHAH, P. S., FAN, L. T., KAO, I. C. & ERICKSON, L. E. 1972 Modeling of growth processes with two liquid phases: A review of drop phenomena, mixing, and growth. *Adv. Appl. Microbiol.* **15**, 367–414.

SPENGLER, J. D. & GOKHALE, N. R. 1973 Drop impactions. *J. Appl. Met.* **12**, 316–321.

VASENIN, I. M., ARKHIPOV, V. A., BUTOV, V. G., GLAZUNOV, A. A. & TROFIMOV, V. F. 1986 Gas dynamics of two phase flow in nozzles. TOMSK University Press.

WASAN, D. T. & MALHOTRA, A. K. 1986 Thin liquid surfactant film drainage phenomena – a review. In *Thin Liquid Film Phenomena* (ed. W. B. Krantz, D. T. Wasan & R. K. Jain). AIChE Symposium Series B, vol. 82 (252), pp. 5–13.

WEINBAUM, S., CHEN, L. & GANATOS, P. 1989 Elastohydrodynamic collision and rebound of a flat plate from a planar surface due to body and fluid inertia. *Phys. Fluids* A **1**, 140–155.